Evolution of geometric phase and explaining the geodesic rule

Hagen, Nathan; Garza-Soto, Luis

DOI
10.1364/JOSAA.538106

Publication date
2024

Document Version
Final published version

Published in
Journal of the Optical Society of America A: Optics and Image Science, and Vision

2014 Vol. 41, No. 11 / November 2024 / Journal of the Optical Society of America A Research Article

Journal of the Optical Society of America A

OPTICS, IMAGE SCIENCE, AND VISION

Evolution of geometric phase and explaining the geodesic rule

NATHAN HAGEN[1,*] AND LUIS GARZA-SOTO[1,2]

[1]Department of Optical Engineering, Utsunomiya University, 7-2-1 Yoto, Utsunomiya, Tochigi, 321-8585, Japan
[2]Department of Aerospace Structures and Materials, Delft University of Technology, Kluyverweg 1, 2629 HS, Delft, The Netherlands
*nh@hagenlab.org

Received 1 August 2024; revised 11 September 2024; accepted 11 September 2024; posted 12 September 2024; published 2 October 2024

We use the recently developed wave model of geometric phase to track the continuous evolution of geometric phase as a wave propagates through optical elements and throughout an optical system. By working directly with the wave properties, we encounter a natural explanation of why the conventional Poincaré sphere solid angle method must use geodesic paths rather than the physical paths of the polarization state—the "geodesic rule"—and show that the existing rules for the solid angle algorithm are incomplete. Finally, we use the physical model to clarify the differences between the Pancharatnam connection and the geometric phase of a wave.

https://doi.org/10.1364/JOSAA.538106

1. INTRODUCTION

The existing literature generally defines geometric phase by cycles of states [1]. Since the phase of a wave is gauge-dependent (depends on our choice of basis for the polarization states) [2], the phase value contains an arbitrary offset [3]. However, if we consider cyclical operations that return a polarized wave to its starting state, then the phase remaining after a full cycle is no longer gauge-dependent. The arbitrary offset cancels out regardless of the choice of basis, and what remains has been commonly referred to as the geometric phase [4].

Some researchers have used the existing theoretical framework to define the geometric phase for an open path [5–7] by determining the phase corresponding to "closing" the path into a cycle. This process, however, leaves it unclear what the geometric phase in such an open path physically represents. We have previously shown [8] that the geometric phase γ can be defined such that it has a value for any wave at any point along its propagation through a system—a quantity that continuously evolves according to its interactions with optical elements and according to coordinate transformations. With this new definition, the change in γ between the starting and ending points of any cycle of states, $\Delta\gamma = \gamma_{\text{end}} - \gamma_{\text{start}}$, is then what most of the existing literature refers to as the geometric phase [9] but that we regard as the *change* in geometric phase. In the discussion below, we show why this generalized definition is useful—that it provides richer information about the physical behavior of the wave, while retaining the previous cyclical state information as a subset.

The most commonly used method for quantifying the geometric phase for a cyclical sequence of polarization states is to draw the sequence of states on the Poincaré sphere, connect each state in the cycle using geodesic curves, and calculate the solid angle subtended by the resulting path [10]. The geometric phase (γ, in radians) is then given by half the solid angle (Ω, in steradians): $\Delta\gamma = -\Omega/2$, for paths traced in a clockwise sense [7]. For paths traced in an anticlockwise sense, $\Delta\gamma = +\Omega/2$. This recipe for calculating $\Delta\gamma$, however, also contains a number of rules.

1. The solid angle is calculated by tracing a geodesic curve between the polarization states before entering and after leaving each homogeneous optical element, even when this geodesic is not the actual path followed by the polarization state as it traverses the element. This is the "geodesic rule" [7,11,12].
2. For the case of inhomogeneous optical elements, such as a cholesteric liquid crystal waveplate (which is a linear retarder with an azimuth angle that rotates continuously along the propagation direction), the geodesic rule no longer holds, and the solid angle is calculated using the actual physical path of the polarization state [13].
3. One must choose the shortest geodesic [11,12,14,15]. For cases in which one can choose from among multiple equally short geodesics in order to close a path, one must choose the one that coincides with the physical path if such a physical path exists [16].

For the first time, the newly developed wave model for geometric phase [8] allows us to explain why these rules exist for the solid angle approach not just mathematically but in terms of a physical model of the wave. Using the wave model operating on the electromagnetic wave vector obtained from Jones calculus, we validate the often stated principle that geodesics are paths

along which γ does not accumulate phase [15,16]. Along the way, we demonstrate that the above rules are incomplete—that we need to add a new fourth rule:

4. If two adjacent optical elements in the wave's path share the same eigenbasis, then they must be combined into a single element for the purpose of calculating Ω.

We also show that the rule of choosing the shortest geodesic is not always true, though the phase wrapping behavior of geometric phase means that one often cannot measure the difference between choosing the shortest and longest geodesic.

In contrast to the differential geometry approach typically used for geometric phase [2,17–20], our analysis below uses only the Jones calculus and simple basis transformations so that γ retains a clear physical meaning at each step, and explicitly shows how to quantify γ's basis dependence.

2. ANALYZING POLARIZATION TRANSFORMATIONS WITHOUT PROPAGATION PHASE

In order to trace the evolving polarization state and geometric phase of a wave propagating through a sequence of optical components, we need to make sure that our model eliminates the effects of propagation phase, leaving only geometric effects. This will allow us to model the smooth change in γ as a wave passes through a linear retarder. For the first time, we will be able to see how the geometric phase evolves as it passes through these elements, and not only at the points just before entering and just after leaving an element. As we will see, there can be a lot going on between these two points.

For a wave's polarization state, we use the electric field vector

$$\mathbf{E} = \begin{pmatrix} A_1 e^{i\phi_1} \\ A_2 e^{i\phi_2} \end{pmatrix}, \tag{1}$$

where A_1 and A_2 are the wave amplitudes, and ϕ_1 and ϕ_2 the corresponding wave phases, along each of two orthogonal basis directions 1 and 2. Although the most common choice of basis is x-y, we will make use of other polarization bases too.

In order to simplify notation when passing through a sequence of standard polarization states, we will use the following letters to represent the corresponding states:

H: horizontally (0° linear) polarized,
V: vertically (90° linear) polarized,
D: diagonally (45° linear) polarized,
A: antidiagonally (−45° linear) polarized,
R: right-circularly polarized,
L: left-circularly polarized,
E: any elliptically polarized.

On the Poincaré sphere representation of polarization states, each pair of orthogonal states **HV**, **DA**, and **RL** occurs at the opposing points on the sphere along a given axis, as shown in Fig. 1(a). To prevent clutter, the figure only shows one of each pair of states along each axis.

In the wave model for geometric phase, the geometric phase γ of a polarized wave, expressed in terms of its two orthogonal components, can be written as [8]

$$\tan(2\gamma) = \frac{A_1^2 \sin(2\phi_1) + A_2^2 \sin(2\phi_2)}{A_1^2 \cos(2\phi_1) + A_2^2 \cos(2\phi_2)}, \tag{2}$$

where γ represents the position of the wave peak relative to the axis that we have defined as our phase reference. Orientation angles are defined with respect to the positive x-axis, so that a wave has zero phase if it reaches its maximum amplitude when its electric field vector is aligned to the x-axis.

In the existing literature, another approach to calculating the geometric phase is to use Pancharatnam's connection to give the difference in phase between the input state $\mathbf{E}_a$ and the evolving state $\mathbf{E}_b$ [3,7,10,16,21,22]:

$$\gamma_p = \arg\left\{\mathbf{E}_a^{\top} \mathbf{E}_b^{*}\right\}. \tag{3}$$

Although this gives a value that is superficially similar to that of Eq. (2), we will see in Section 4 that in fact γ and γ_p represent different things.

When a polarization state passes through a birefringent optical element, the state is transformed according to the element's Jones matrix. For example, the matrix of a linear retarder has the form [23]

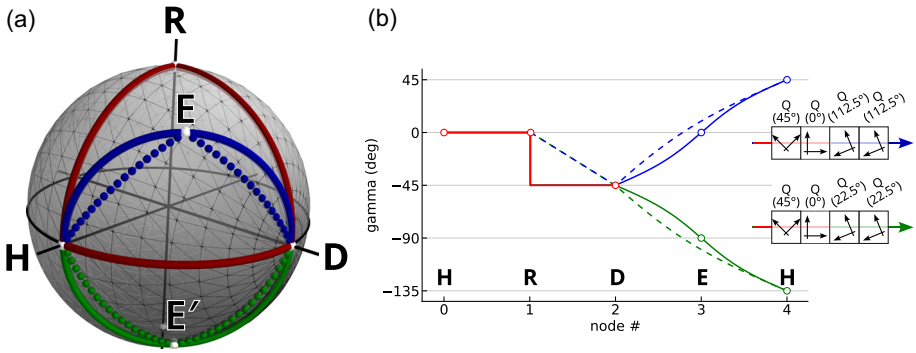

Fig. 1. (a) Sequence #1: **H**–**R**–**D**–**H**. The first two (red) path segments are performed with QWPs oriented at 45° and 0°. The third segment of the cyclical path is performed using (blue) two QWPs with fast axis at 112.5°, or (green) two QWPs with fast axis at 22.5°. The dotted green and blue paths show the geodesic curves from **D** to **E** (the midpoint) and then from **E** to **H**. (b) The calculated geometric phase for both paths, (solid curves) using Eq. (2) in the **HV** basis, (dashed curves) using the Pancharatnam connection Eq. (3). The green path is unwrapped at the $-\pi/2$ boundary in order to clearly illustrate its symmetry with the blue path. (b) (inset) The two different optical systems used for the two paths modeled.

$$\mathbf{LR}(\theta, \delta, \Phi) = e^{i\Phi}\left[\mathbf{R}(-\theta)\begin{pmatrix} e^{-i\delta/2} & 0 \\ 0 & e^{+i\delta/2}\end{pmatrix}\mathbf{R}(\theta)\right] \quad (4)$$

$$= e^{i\Phi}\begin{pmatrix} e^{-i\delta/2}\cos^2\theta + e^{i\delta/2}\sin^2\theta & (e^{-i\delta/2} - e^{i\delta/2})\cos\theta\sin\theta \\ (e^{-i\delta/2} - e^{i\delta/2})\cos\theta\sin\theta & e^{i\delta/2}\cos^2\theta + e^{-i\delta/2}\sin^2\theta\end{pmatrix}, \quad (5)$$

where δ is the retardance. The operator $\mathbf{R}(\theta)$ represents a rotation matrix:

$$\mathbf{R}(\theta) = \begin{pmatrix}\cos\theta & -\sin\theta \\ \sin\theta & \cos\theta\end{pmatrix}. \quad (6)$$

The angle θ is the orientation angle of the element's axis with respect to the x-axis. For a retarder, this is the retarder's fast axis angle. The central matrix in Eq. (4) represents a linear retarder in its eigenbasis, so that its fast axis azimuth is oriented along the first eigenstate.

In Eqs. (4) and (5), Φ is the propagation phase—the mean phase accumulated by the wave upon propagating through the element. For any given Jones matrix, the propagation phase is calculated as the average of the phases accumulated by each of the eigenstates (the eigenpolarizations). This is equal to the phase accumulated by passing through an equivalent glass plate of the same refractive index,

$$\Phi = \frac{1}{2}\sum_j 2\pi n_j \ell/\lambda, \quad (7)$$

for refractive index n, plate thickness ℓ, wavelength λ, and j representing e or o for the ordinary or extraordinary index.

Although there are different forms for the Jones matrices, when working with geometric phase it is important to use a definition of the Jones matrices in which the propagation phase can be removed, so that only geometric components remain. Thus, in our work below we set $\Phi = 0$, and allow the phases to operate symmetrically on the element's eigenstates—the "symmetric phase convention" [23].

Setting $\Phi = 0$ is a valid procedure because it is effectively the way that these phases are measured interferometrically—as a difference between a reference beam phase and a sample beam phase. When measuring with coherent light, it is not possible to measure the relative phase $\Delta\Phi = \Phi_{\text{sample}} - \Phi_{\text{ref}}$ from the interferogram. Instead, one measures the change in the interferogram phase as a function of a parameter adjusted in the sample arm. With low coherence light, one can measure $\Delta\Phi$ by locating the middle of the coherence envelope, in which case it is not difficult to separate out propagation phase (which moves the coherence envelope) from geometric phase (which does not move the envelope) [24].

An important property of the rotation and retarder Jones matrices that we will use is that their parameters are additive on matrix concatenation. That is, if we concatenate N retarders, each with δ/N retardance, then the concatenated system will be equivalent to a single retarder matrix with retardance δ:

$$\mathbf{LR}(\theta, \delta) = \prod_n \mathbf{LR}(\theta, \delta/N), \quad (8)$$

and the same additive property holds for rotation matrices:

$$\mathbf{R}(\theta) = \prod_n \mathbf{R}(\theta/N). \quad (9)$$

Thus, if we want to know how the polarization state evolves as it propagates inside a linear retarder, then we can split the retarder into many thin retarder elements, and analyze the polarization state after passing through each thin element. In the limit of $N \to \infty$, the matrices represent differential elements [13,25].

3. TRACKING GEOMETRIC PHASE ALONG A PATH USING THE JONES CALCULUS

To illustrate our method for tracking geometric phase evolution, we first consider transformations of a wave with horizontal polarization state **H** passing through an optical system, and we analyze the geometric phase γ as it propagates through this system. The system consists of four quarter-waveplate (QWP) elements: one QWP with the fast axis oriented at 45°, followed by a second QWP oriented at 0°, and finally by a pair of QWPs that are either oriented at 112.5° (blue path) or 22.5° (green path). The resulting paths of polarization states are drawn on the Poincaré sphere in Fig. 1(a). The geometric phase at each point along the polarization state's evolution as it passes through this system is shown in Fig. 1(b). The red path shows the polarization state starting at **H**, rotating up to the pole at **R**, rotating again to **D**, and finally returning to **H** along either the blue or green curve. Each nonadiabatic change in a path is considered a node, represented by a small white dot. However, as we will see below, the node placed halfway along the blue and green curves, indicating the state between the two QWPs, is an adiabatic point. If we temporarily ignore this node, as we would do if we used HWPs in place of pairs of QWPs, then we could observe that even though the blue and green paths traverse different physical polarization paths, they traverse the same sequence of nodes.

In the common approach used by the existing literature, the geometric phase produced by traversing this path is calculated by connecting the various nodes by geodesic arcs. The solid angle Ω subtended by the area inside the curve leads to $\gamma = -\Omega/2$ [26]. In one of the example paths shown in Fig. 1, the node-connected path segments trace a spherical triangle shown by three red curves. This triangle encloses a solid angle of $\Omega = \pi/2$ steradians, giving $\gamma = -\pi/4$. (In order to clearly differentiate the various phases and angles, orientation angles will always be stated in degrees, while geometric phases will be given in radians. An exception is made for the figures, where using degrees for γ is more natural.)

Next we consider the same path, calculated instead using the wave model. For this approach, we create an input Jones vector representing the horizontal polarization state, in the canonical x-y basis: $\mathbf{E_H} = \binom{1}{0}$. We then split each of the optical components into a series of thin elements and record the polarization state at each step as it passes through the system. Thus, we obtain a sequence of polarization states representing steps along the curves between nodes and also the nodes themselves. For each state, we calculate γ using Eq. (2), with the result shown in Fig. 1(b). From the figure, we can see that the phase starts at zero at state **H**, suddenly decreases to −45° as it leaves **R**, and stays at −45° as it reaches **D**, but after this splits in two directions depending on whether the wave travels along the blue or green path, reaching either +45° or −135° at the end.

In order to see how the geometric phase arises from the various operations, we can analyze the wave phase directly from the polarization state vector. At each optical element, we make sure that the polarization state transformation matrix contains no propagation phase, so that any changes to the state are purely due to geometric effects.

The path going from the initial state **H** towards **R** uses a QWP with the fast axis oriented at 45°, which means that the eigenbasis for this QWP is the pair of states **D** and **A**. If we represent the horizontal input state in the **DA** basis, then we have

$$\mathbf{E_{DA}} = \frac{1}{\sqrt{2}}\begin{pmatrix} 1 & 1 \\ -1 & 1 \end{pmatrix} \cdot \mathbf{E_{HV}} = \frac{1}{\sqrt{2}}\begin{pmatrix} 1 \\ -1 \end{pmatrix}, \tag{10}$$

where $\mathbf{E_{HV}}$ is the input electric field vector represented in the **HV** basis, and $\mathbf{E_{DA}}$ the same field represented in the **DA** basis.

In the eigenbasis, the Jones matrix of the retarder is simply

$$\mathbf{LR}(\delta, 0) = \begin{pmatrix} e^{-i\delta/2} & 0 \\ 0 & e^{+i\delta/2} \end{pmatrix}, \tag{11}$$

which clearly contains no propagation phase. Applying this matrix to the input state produces

$$\mathbf{E'_{DA}} = \begin{pmatrix} e^{-i\delta/2} & 0 \\ 0 & e^{+i\delta/2} \end{pmatrix} \cdot \frac{1}{\sqrt{2}}\begin{pmatrix} 1 \\ -1 \end{pmatrix} = \frac{1}{\sqrt{2}}\begin{pmatrix} e^{-i\delta/2} \\ -e^{+i\delta/2} \end{pmatrix}, \tag{12}$$

for retardance δ. The state of polarization slowly evolves as the wave passes through the retarder, eventually reaching $\delta = \pi/2$ for a QWP, so that the polarization state exiting the retarder becomes

$$\mathbf{E'_{DA}} = \frac{1}{\sqrt{2}}\begin{pmatrix} e^{-i\pi/4} \\ e^{-i3\pi/4} \end{pmatrix} = \frac{e^{-i\pi/4}}{\sqrt{2}}\begin{pmatrix} 1 \\ -i \end{pmatrix}. \tag{13}$$

This is the state **R** represented in the **DA** basis. Figure 2 shows the amplitudes and phases of the two components of the Jones vector along the polarization state path—these curves help to visualize the relative positions of the component waves that determine the location of the composite polarized wave peak and therefore its geometric phase. In the next step of the sequence, going from **R** to **D**, the light passes into a QWP with the fast axis oriented at 0°. In this case, the eigenbasis is **HV**, and so we translate our Jones vector back into the canonical basis:

$$\mathbf{E_{HV}} = \frac{1}{\sqrt{2}}\begin{pmatrix} 1 & -1 \\ 1 & 1 \end{pmatrix} \cdot \mathbf{E'_{DA}} = \frac{1}{\sqrt{2}}\begin{pmatrix} 1 \\ -i \end{pmatrix}. \tag{14}$$

Since the two components of the polarization vector have the same amplitude, the geometric phase will be halfway between the two vector component phases, so that now $\gamma = -\pi/4$, in agreement with the curve drawn in Fig. 1(c). In this basis, the second retarder's matrix is given by Eq. (11), so that the curve between nodes **R** and **D**, expressed in the **HV** basis, is

$$\mathbf{E'_{HV}} = \begin{pmatrix} e^{-i\delta/2} & 0 \\ 0 & e^{+i\delta/2} \end{pmatrix} \cdot \frac{1}{\sqrt{2}}\begin{pmatrix} 1 \\ -i \end{pmatrix} = \frac{1}{\sqrt{2}}\begin{pmatrix} e^{-i\delta/2} \\ -ie^{+i\delta/2} \end{pmatrix}. \tag{15}$$

Substituting $\delta = \pi/2$ for the QWP gives the polarization state at the exit surface of the retarder as

$$\mathbf{E'_{HV}} = \frac{e^{-i\pi/4}}{\sqrt{2}}\begin{pmatrix} 1 \\ 1 \end{pmatrix}. \tag{16}$$

Although the electric field vector itself has zero phase, the global phase factor shifts the entire wave by $-\pi/4$. Thus, in the **HV** basis, we can see that the geometric wavefront for state **D** is $\gamma = -\pi/4$. Once again, by viewing the transformation from the perspective of the eigenbasis (the geodesic curve's axis of symmetry), we find that the phase is unchanged. (Note, however, that since our polarization state has changed from our original **H**, the phase measured by an interferometer in this case will not be equal to γ [8].)

Now that we have reached state **D**, the final segment of the path involves using a pair of QWPs to rotate the state from **D** back to its original state **H**. Starting with the polarization state at node **D**, we translate the state into the eigenbasis of the retarder (in this case, linear polarization oriented at either 112.5° or 22.5°) and apply the retardance Eq. (4). Starting with the blue path drawn in Fig. 1, we choose the QWPs oriented at 112.5°. We translate the polarization vector at **D** into this retarder's eigenbasis as

$$\begin{aligned}\mathbf{E}_{112} &= \begin{pmatrix} \cos\left(\frac{5\pi}{8}\right) & \sin\left(\frac{5\pi}{8}\right) \\ -\sin\left(\frac{5\pi}{8}\right) & \cos\left(\frac{5\pi}{8}\right) \end{pmatrix} \cdot \frac{e^{-i\pi/4}}{\sqrt{2}}\begin{pmatrix} 1 \\ 1 \end{pmatrix} \\ &= \frac{e^{-i\pi/4}}{\sqrt{2}}\begin{pmatrix} \cos\left(\frac{5\pi}{8}\right) + \sin\left(\frac{5\pi}{8}\right) \\ -\sin\left(\frac{5\pi}{8}\right) + \cos\left(\frac{5\pi}{8}\right) \end{pmatrix}. \end{aligned} \tag{17}$$

Next we apply the retardance. For a HWP in its eigenbasis, the retarder matrix has the simple form of $\mathbf{LR}(\pi/2, 0) = \begin{pmatrix} -i & 0 \\ 0 & i \end{pmatrix}$ so that the polarization vector becomes

$$\begin{aligned}\mathbf{E'_{112}} &= \begin{pmatrix} -i & 0 \\ 0 & i \end{pmatrix} \cdot \frac{e^{-i\pi/4}}{\sqrt{2}}\begin{pmatrix} \cos\left(\frac{5\pi}{8}\right) + \sin\left(\frac{5\pi}{8}\right) \\ -\sin\left(\frac{5\pi}{8}\right) + \cos\left(\frac{5\pi}{8}\right) \end{pmatrix} \\ &= \frac{ie^{-i\pi/4}}{\sqrt{2}}\begin{pmatrix} -\cos\left(\frac{5\pi}{8}\right) - \sin\left(\frac{5\pi}{8}\right) \\ \cos\left(\frac{5\pi}{8}\right) - \sin\left(\frac{5\pi}{8}\right) \end{pmatrix}. \end{aligned} \tag{18}$$

Finally, translating this back into the **HV** basis gives

$$\mathbf{E_{HV}} = \begin{pmatrix} \cos\left(\frac{5\pi}{8}\right) & \sin\left(\frac{5\pi}{8}\right) \\ -\sin\left(\frac{5\pi}{8}\right) & \cos\left(\frac{5\pi}{8}\right) \end{pmatrix} \cdot \mathbf{E'_{112}} = e^{+i\pi/4}\begin{pmatrix} 1 \\ 0 \end{pmatrix}. \tag{19}$$

This is the result for the blue path. Following a similar procedure for the green path, using $\theta = 22.5°$ in place of the above $\theta = 112.5°$, we get the result

$$\mathbf{E_{HV}} = e^{-i3\pi/4}\begin{pmatrix} 1 \\ 0 \end{pmatrix}. \tag{20}$$

In both cases, the polarization state vectors have no phase, so that the global phase factor by itself determines the phase shift. We can see that there is a $\Delta\gamma = \pi$ difference in geometric phase between the blue and green paths, matching the γ curves drawn in Fig. 1(b).

According to the standard theory, the physical path traversed between nodes has no effect on the geometric phase calculation, but in the situation of the blue and green curves of Fig. 1, we see that it can be ambiguous about which geodesic to choose. The evolution curves clearly show that the two should be π radians out of phase, which indicates that the solid angle approach

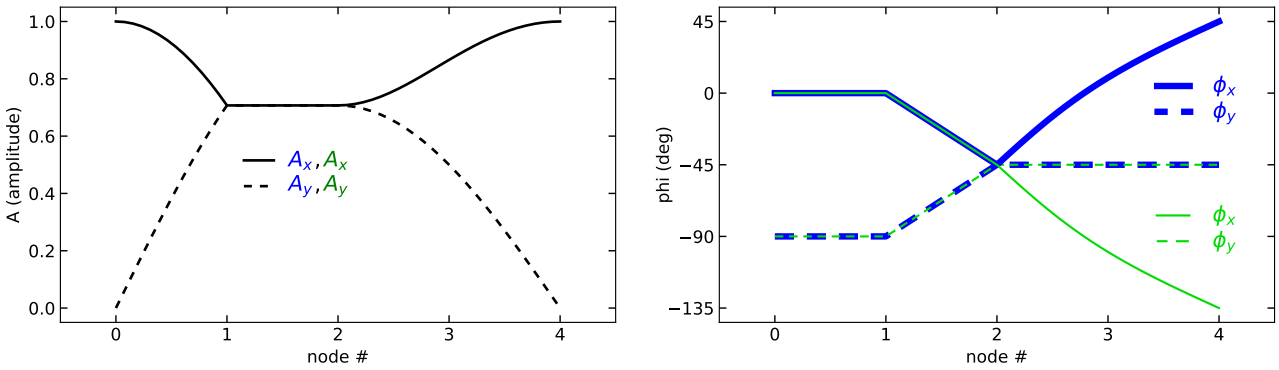

Fig. 2. The amplitudes and phases of the x and y components of the Jones vector, for the polarization state paths of Fig. 1. The blue and green colors represent the blue and green paths of Fig. 1. While amplitudes (A_x, A_y) and the phase ϕ_x of the blue and green paths are the same, ϕ_y is different.

in this case should choose the longer geodesic between the nodes—the one following the equator along the back side of the sphere—and not the shorter geodesic that most would require. A little-known fifth rule for the solid angle calculation is needed to remove this ambiguity, though we have only seen it expressed in Refs. [21] and [26]: in order to determine which geodesic is the correct one to choose, we should calculate the geometric phase for the physical polarization state path as it slowly approaches the final state (the blue or the green curve of Fig. 1).

The π radians phase difference in γ between the blue and green paths has physical meaning: the two paths experience the final HWP with the fast and slow axes swapped. As shown in Fig. 2, while the wave amplitudes for the two paths remain the same, ϕ_x increases to $+\pi/4$ for the blue path, and $-3\pi/4$ for the green path, and thus there is a π phase difference between the two paths' ϕ_x values due to the two waveplate orientations.

Another observation we can make about the paths drawn in Fig. 1(a) is that since there are two QWPs here rather than a single HWP, the current geodesic rule would require one to draw a geodesic connecting the states at the entrance and exit of the first QWP, and another geodesic at the entrance and exit of the second QWP. These are the paths drawn with dotted green and blue geodesic curves in Fig. 1(a). However, if we incorporate these intermediate geodesic curves in our calculation of the solid angle, we obtain $\Omega_{\text{blue}} = 0.892$ rad and $\Omega_{\text{green}} = 2.25$ rad, rather than the known correct values of $\Omega = \pi/2$. Thus, in order to get the correct answer using the geodesic rule, we instead need to add a new rule (#4): if the path includes multiple adjacent elements that share an eigenbasis, then these elements must be combined into a single entity, so that the geodesic curve is therefore drawn from the entering state to exit state of that entire subsystem, rather than between each individual optical element. In the wave model Eq. (2), these special rules are not needed.

4. WAVE GEOMETRIC PHASE AND INTERFEROMETER PHASE

The geometric phase evolution curves drawn in Fig. 1 show two separate sets of trajectories: one set (solid curves) drawn using the wave model Eq. (2) evaluated in the fixed **HV** basis, and another set (dashed curves) drawn using the Pancharatnam connection Eq. (3) with respect to the input state and the evolving state. Although the two curves show very similar values and behavior, they do not in general coincide except at the nodes of the path. (Node **E** is an exception, because it does not represent a change in the polarization eigenbasis of the system.)

In the wave model, the geometric phase γ is given by composing the amplitudes and phase of two polarized wave components (in this case, E_x and E_y) and calculating the location of the wave peak with respect to the peak of the reference wave (in this case, the E_x wave). As the wave propagates through the system, the x- and y-component waves undergo changes in amplitude and phase that cause shifts in the location of the composite polarized wave peak relative to the reference wave's peak. This shift is γ as given by Eq. (2).

The Pancharatnam connection, on the other hand, expresses γ_p as the interferogram phase resulting from interfering the input wave, which we can write as $\mathbf{E}_a$, with the polarized wave $\mathbf{E}_b$ [26]. In this case, since the input state is **H**, E_a is the same as the reference wave of the wave model, i.e., E_x. Moreover, the wave peak location of the polarized wave $\mathbf{E}_b$ is exactly what the wave model delivers, and so one can easily slip into thinking that the two are the same. The difference, however, is that γ models the peak location of a *single wave*, whereas γ_p represents the phase that results from interfering that wave with the reference wave. As mentioned in Ref. [8] (Section 6), these will not always coincide. In particular, the Pancharatnam connection considers interfering two waves of differing polarization states, and this causes a shift in the location of the interferogram phase away from the location coinciding with the sample arm's geometric phase. Thus, we can say that the wave model delivers the geometric phase of the wave itself, while the Pancharatnam connection delivers the interferogram geometric phase.

It is also possible to pose the problem in such a way that the two methods of calculation [Eqs. (2) and (3)] coincide. If we represent the wave components $\mathbf{E}_1$ and $\mathbf{E}_2$ used in Eq. (2) in terms of the evolving system eigenbasis rather than the fixed **HV** basis, then we find that $\gamma = \gamma_{\text{p}}$.

Although it can be confusing to think of the geometric phase for an evolving basis, one advantage of using this rather than a fixed basis is that it prevents having jump discontinuities in the evolution curve, as shown in Fig. 1. In a fixed basis, jump discontinuities can occur either when one of the component

amplitudes (A_1 or A_2) approaches zero, or where the denominator of Eq. (2) approaches zero. For the **HV** basis, this occurs at the **R** and **LL** states, which is why the red curve in Fig. 1 has a jump discontinuity as it passes through state **R**.

On the other hand, a significant benefit to using the wave model is that it makes the basis dependence of γ explicit through the necessity of having to choose wave components E_1 and E_2. That is, in order to calculate γ via Eq. (2), we are forced to choose an orthogonal basis in which to represent the wave, giving parameters (A_1, ϕ_1) and (A_2, ϕ_2).

5. WHY THE GEODESIC RULE WORKS

Figure 3(a) shows another sequence of polarization states traced on the Poincaré sphere. As in Section 5, the paths are generated by slicing each polarization component into hundreds of thin elements, and calculating the polarization state exiting each thin element. In Fig. 3(a), we start with a right-circular polarization state **R** and use a HWP oriented at $\theta = -45°$ to convert this into **L**. From there we use a second HWP to return to **R**, but choose a variety of different orientation angles to do so. The figure shows paths for HWPs with fast-axis orientation angles θ from $+45°$ to $+135°$ at intervals of $11.25°$. Figure 3(b) shows the corresponding evolution curves for γ calculated from Eq. (2)—the geometric phase calculated from the perspective of the **HV** basis.

Following the polarization state evolution with the Jones calculus, we start with the state at **R** written in the **HV** basis,

$$\mathbf{E}_{\mathbf{HV}} = \frac{1}{\sqrt{2}}\begin{pmatrix} 1 \\ -i \end{pmatrix}, \tag{21}$$

which has $\gamma = -\pi/4$. The first HWP has its fast axis oriented at $-45°$, so that we start by projecting the above state onto the antidiagonal-diagonal **AD** basis:

$$\mathbf{E}_{\mathbf{AD}} = \begin{pmatrix} \cos\left(\frac{-\pi}{4}\right) & \sin\left(\frac{-\pi}{4}\right) \\ -\sin\left(\frac{-\pi}{4}\right) & \cos\left(\frac{-\pi}{4}\right) \end{pmatrix} \cdot \frac{1}{\sqrt{2}}\begin{pmatrix} 1 \\ -i \end{pmatrix} = \frac{1}{2}\begin{pmatrix} 1+i \\ 1-i \end{pmatrix}. \tag{22}$$

(While all of these operations can be performed in a constant basis, switching to each element's eigenbasis provides a clearer analysis.) Note that the **AD** basis differs from the **DA** basis in that the former is rotated by $90°$ with respect to the latter, as needed in order to keep the first polarization basis vector oriented along the waveplate's fast axis.

Now that we are in the HWP's eigenbasis, applying its retardance to the state gives

$$\mathbf{E}'_{\mathbf{AD}} = \begin{pmatrix} -i & 0 \\ 0 & i \end{pmatrix} \cdot \frac{1}{2}\begin{pmatrix} 1+i \\ 1-i \end{pmatrix} = \frac{1}{2}\begin{pmatrix} 1-i \\ 1+i \end{pmatrix}. \tag{23}$$

The two components of this state, $1-i$ and $1+i$, correspond to phases of $+45°$ and $-45°$. Since the amplitudes of the two are equal and the two phases are symmetric about zero, Eq. (2) gives a geometric phase of zero for this state in this basis.

In the next step, we use a HWP whose orientation angle θ is not fixed, but we can use the angle as a variable in our basis transformation of the polarization state to obtain

$$\mathbf{E}_\theta = \begin{pmatrix} \cos\left(\theta+\frac{\pi}{4}\right) & \sin\left(\theta+\frac{\pi}{4}\right) \\ -\sin\left(\theta+\frac{\pi}{4}\right) & \cos\left(\theta+\frac{\pi}{4}\right) \end{pmatrix} \cdot \mathbf{E}'_{\mathbf{AD}} = \frac{e^{i\theta}}{\sqrt{2}}\begin{pmatrix} 1 \\ i \end{pmatrix}. \tag{24}$$

Here we see that the state acquires a phase of $\theta + \frac{\pi}{4}$ as a result of the basis transformation. Now that we are in the HWP's eigenbasis, we apply its retardance with

$$\mathbf{E}'_\theta = \begin{pmatrix} -i & 0 \\ 0 & i \end{pmatrix} \cdot \frac{e^{i\theta}}{\sqrt{2}}\begin{pmatrix} 1 \\ i \end{pmatrix} = \frac{e^{i\theta}}{\sqrt{2}}\begin{pmatrix} -i \\ -1 \end{pmatrix}. \tag{25}$$

Finally, we project this last state onto the **HV** basis:

$$\mathbf{E}_{\mathbf{HV}} = \begin{pmatrix} \cos(-\theta) & \sin(-\theta) \\ -\sin(-\theta) & \cos(-\theta) \end{pmatrix} \cdot \mathbf{E}'_\theta = \frac{-ie^{i2\theta}}{\sqrt{2}}\begin{pmatrix} 1 \\ -i \end{pmatrix}. \tag{26}$$

We see that if the return path uses a HWP oriented at $+45°$, then the wave phase will be the same as our starting phase. This is as we expect, since this path subtends no solid angle. However, if the return path uses a HWP oriented at $90°$, then we find that the wave phase has shifted by $+90°$ from our starting point, in agreement with the solid angle approach to calculating γ, namely, that $\Delta\gamma = 2\theta$.

This procedure reinforces the often-stated feature of geometric phase that γ does not accumulate along geodesic paths. Indeed, in the case of Fig. 3, where the two components of the polarization state always keep the same amplitude in the

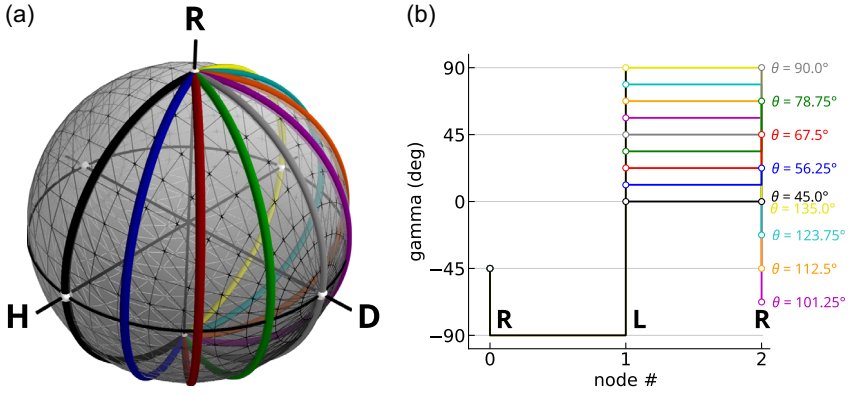

Fig. 3. Sequence #2: (a) path **R**–**L**–**R**. The first segment from **R** to **L** is performed with a HWP oriented at $-45°$. The second segment returning from **L** to **R** is performed with any one of HWPs whose fast axes are oriented at $11.25°$ intervals starting from $+45°$. (b) The calculated geometric phase for each path.

bases that we use, all of the geometric phase is produced by the basis transformations themselves. This points to one way of interpreting the "geodesic rule" in the solid angle approach to calculating γ. The reason we need to link nodes in the path using geodesic curves rather than physical curves, in the case of Fig. 3 at least, is that all of the action occurs at the nodes. Viewed in the eigenbasis of a retarder, the polarization state may evolve as it propagates through the retarder, but the geometric phase does not. The separation of the two eigenwaves as they emerge from the retarder, as transformed by any change of basis, induces the shift in wave phase with respect to the phase reference plane.

The special thing about homogeneous optical elements (whose physical paths are to be replaced by geodesics under the geodesic rule) is that the eigenbasis does not change between the point where we enter and leave the element or set of elements. For the geodesic rule to work, we must delay evaluating the polarization state until we emerge from the eigenbasis and are ready to transform the state to a new basis—as indicated by a node in the path.

6. EXAMPLE OF DIFFERENT PHYSICAL PATHS PRODUCING THE SAME γ

Figure 4 shows a pair of paths created with a series of HWPs to loop the polarization state around the Poincaré sphere. In one path, each successive HWP has its fast axis rotated by 45° with respect to the previous HWP. In the second path, the fast axis is incremented by 22.5°, creating smaller loops on the sphere. In the conventional solid angle approach to analyzing these paths, the curves connecting the path nodes will all lie along the equator, rather than following the physical polarization state. And in the conventional approach, it is only once the paths return to their starting point, when they close the cycle, that the geometric phase can finally be defined. For both of these paths, this $\Delta\gamma$ will be zero or π because all of the nodes on the path lie on the same great circle. However, in the evolution curves of Fig. 4(b), we can see that there is a lot of activity occurring in the geometric phase along these paths, but that once we return to state **H** we get $\Delta\gamma = \gamma_{\text{end}} - \gamma_{\text{start}} = n\pi$ for $n \in \{0, 2, 4\}$, in agreement with conventional theory. (In this case, if we are using phase wrapping then $n = 0$ for both paths. If unwrapping the phase, then we find that $n = 2$ for the red path, and $n = 4$ for the blue path.)

The γ evolution curves of Fig. 4 show that the blue curves exhibit phase changes that are twice as fast as those of the red curves, that is, twice as fast when described in terms of the geometric phase accumulated for a given polarization state azimuth angle. Thus, for example, the first node of the red curve lies at **D**, which coincides with the polarization state at the second blue curve node. If we draw a geodesic between the starting and ending points, we would use the exact same geodesic for the two curves, but the γ of the blue curve will be twice the red curve value there. This should probably not surprise, since the blue curves and red ones both use HWPs, and there are twice as many blue ones, so that the blue path will experience twice as much retardance splitting of waves. One can also note that there are small differences in the shapes of the red and blue curves between nodes, with the red curves showing a larger deviation from linearity.

Following the polarization state evolution with the Jones calculus, we start with the state at **H** and, following the red curve, project the state onto the first HWP's eigenbasis (fast axis oriented at 22.5°):

$$\mathbf{E}_{22} = \begin{pmatrix} \cos\left(\frac{\pi}{8}\right) & \sin\left(\frac{\pi}{8}\right) \\ -\sin\left(\frac{\pi}{8}\right) & \cos\left(\frac{\pi}{8}\right) \end{pmatrix} \begin{pmatrix} 1 \\ 0 \end{pmatrix} = \begin{pmatrix} \cos\left(\frac{\pi}{8}\right) \\ -\sin\left(\frac{\pi}{8}\right) \end{pmatrix}. \quad (27)$$

Applying the halfwave retardance in this basis gives

$$\mathbf{E}'_{22} = \begin{pmatrix} -i & 0 \\ 0 & i \end{pmatrix} \begin{pmatrix} \cos\left(\frac{\pi}{8}\right) \\ -\sin\left(\frac{\pi}{8}\right) \end{pmatrix} = -i \begin{pmatrix} \cos\left(\frac{\pi}{8}\right) \\ \sin\left(\frac{\pi}{8}\right) \end{pmatrix}. \quad (28)$$

Evaluating this state in the **HV** basis, we obtain

$$\mathbf{E}'_{\mathbf{HV}} = \begin{pmatrix} \cos\left(\frac{\pi}{8}\right) & \sin\left(\frac{\pi}{8}\right) \\ -\sin\left(\frac{\pi}{8}\right) & \cos\left(\frac{\pi}{8}\right) \end{pmatrix} \cdot -i \begin{pmatrix} \cos\left(\frac{\pi}{8}\right) \\ \sin\left(\frac{\pi}{8}\right) \end{pmatrix} = -i \begin{pmatrix} 1 \\ 1 \end{pmatrix}, \quad (29)$$

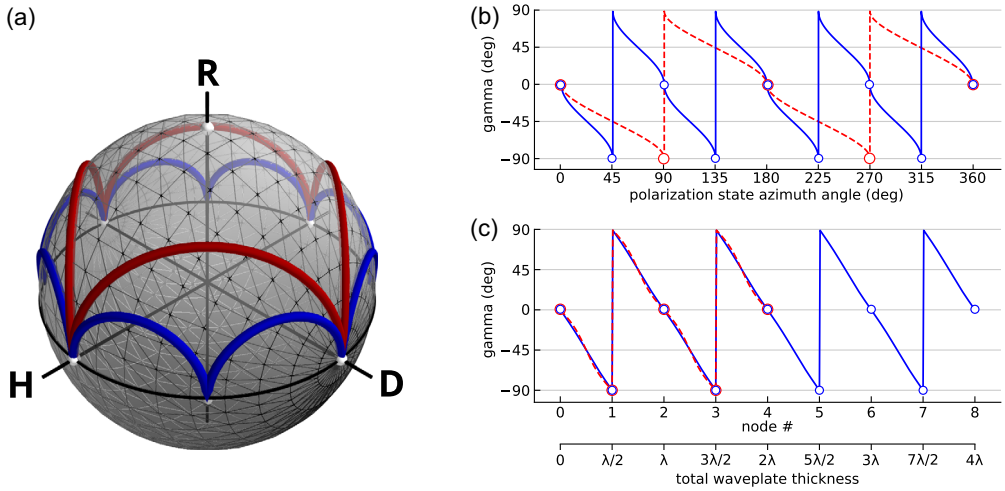

Fig. 4. (a) Sequence #3: two paths that use HWPs to cycle around the Poincaré sphere—one (shown in red) where the orientation angle of each HWP increments by 45° at each node, and another (shown in blue) where the HWP angles increment by 22.5°. The starting state for each path is **H**. (b), (c) The calculated geometric phase for the paths, where (b) and (c) display the same data using different abscissae.

which has a phase shift of $\gamma = -\pi/2$, in agreement with Fig. 4(b), where the 180° has been wrapped to 0°. Since these curves are smooth, we can easily unwrap them to obtain the unwrapped phase if we wish.

Following the same process for the blue curve, the first HWP's eigenbasis is determined by its fast axis oriented at 11.25°. Projecting the state **H** onto this basis gives

$$\mathbf{E}_{11} = \begin{pmatrix} \cos\left(\frac{\pi}{16}\right) & \sin\left(\frac{\pi}{16}\right) \\ -\sin\left(\frac{\pi}{16}\right) & \cos\left(\frac{\pi}{16}\right) \end{pmatrix} \begin{pmatrix} 1 \\ 0 \end{pmatrix} = \begin{pmatrix} \cos\left(\frac{\pi}{16}\right) \\ -\sin\left(\frac{\pi}{16}\right) \end{pmatrix}. \tag{30}$$

Applying the halfwave of retardance in this basis,

$$\mathbf{E}'_{11} = \begin{pmatrix} -i & 0 \\ 0 & i \end{pmatrix} \begin{pmatrix} \cos(\frac{\pi}{16}) \\ -\sin(\frac{\pi}{16}) \end{pmatrix} = -i \begin{pmatrix} \cos(\frac{\pi}{16}) \\ \sin(\frac{\pi}{16}) \end{pmatrix}. \tag{31}$$

Next, we rotate this by 22.5° to project this state onto the 33.75°:123.75° basis:

$$\begin{aligned} \mathbf{E}_{33} &= \begin{pmatrix} \cos\left(\frac{\pi}{8}\right) & \sin\left(\frac{\pi}{8}\right) \\ -\sin\left(\frac{\pi}{8}\right) & \cos\left(\frac{\pi}{8}\right) \end{pmatrix} \cdot -i \begin{pmatrix} \cos\left(\frac{\pi}{8}\right) \\ \sin\left(\frac{\pi}{8}\right) \end{pmatrix} \\ &= -i \begin{pmatrix} \cos\frac{\pi}{8}\cos\frac{\pi}{16} + \sin\frac{\pi}{8}\sin\frac{\pi}{16} \\ -\cos\frac{\pi}{8}\sin\frac{\pi}{16} + \sin\frac{\pi}{8}\cos\frac{\pi}{16} \end{pmatrix}. \end{aligned} \tag{32}$$

Next we apply the halfwave retardance in this basis:

$$\mathbf{E}'_{33} = \begin{pmatrix} -i & 0 \\ 0 & i \end{pmatrix} \cdot \mathbf{E}_{33} = \begin{pmatrix} -\cos\frac{\pi}{16} \\ -\sin\frac{\pi}{16} \end{pmatrix}. \tag{33}$$

And finally we project this state back into the **HV** basis in order to evaluate γ there:

$$\mathbf{E}_{\mathbf{HV}} = \begin{pmatrix} \cos\left(\frac{-3\pi}{16}\right) & \sin\left(\frac{-3\pi}{16}\right) \\ -\sin\left(\frac{-3\pi}{16}\right) & \cos\left(\frac{-3\pi}{16}\right) \end{pmatrix} \cdot \mathbf{E}'_{33} = \frac{-1}{\sqrt{2}} \begin{pmatrix} 1 \\ 1 \end{pmatrix}. \tag{34}$$

Due to the −1 factor in front, we see that this wave is 180° out of phase with respect to our starting point, in agreement with Fig. 4(b).

Although not shown in Figs. 1–4, we have also verified that the Jones calculus approach properly inverts the sign of the geometric phase when the sense of the path is reversed (that is, when the elements are traversed in reverse order). Just as the order of rotations matters when performing rotations in 3D (the 3D rotation group is non-abelian), the order in which polarization transformations are performed affects the phase shift.

7. CONCLUSION

We have shown that the wave model of geometric phase, based on the composition of waves, allows us to visualize how γ is generated, as the shift in the polarized wave peak location as a wave proceeds through an optical system. Because the wave composition approach is agnostic to paths and treats each polarization state independently, it is possible to analyze the continuous evolution of γ as a wave propagates through an optical element, and through any optical system. This approach not only replicates all existing results of cyclical-path geometric phase calculations, it also explains the specific rules under which solid-angle-based calculations of γ must work.

From these new insights, we see that the gauge-dependence of geometric phase plays a critical role in generating phase shifts. As the wave passes from one polarization element to another, if the two elements do not share the same eigenbasis then we see that there can be a sudden phase shift induced by the transition. This explains the need for a "fourth rule" for calculating γ based on solid angles on the Poincaré sphere: any consecutive elements sharing an eigenbasis must be treated as a single element for the purposes of tracing geodesics. This focus on choice of basis also allows us to explain how the Pancharatnam connection's phase γ_p differs from the wave model's γ, and how the meaning of γ_p may differ from what some users imagine it to mean.

The approach of slicing optical elements and tracking γ as it slowly evolves during its propagation can leave the impression that the system is adiabatic. While γ evolves adiabatically between nodes, where the wave is propagating through a homogeneous medium, a node represents a sudden change—either in the first derivative of the phase (a jump) or in the second derivative (a kink in the evolution curve). These sudden changes are induced by correspondingly sudden shifts in the relative amplitudes and phases of the two wave components upon entering a new birefringent optical element.

Finally, the existing literature has often described geometric phase as exhibiting "path memory" [14,27–30]. However, if one considers the path as being the sequence of geodesic curves, then our analysis above has shown that, if we view the path through each successive eigenbasis, then it is not the geodesic curves themselves but rather the basis transformations that occur at path nodes that generate geometric phase. In addition, if one considers the physical path of the polarization state, then Figs. 1 and 4 demonstrate that this path memory is incomplete: there may be multiple physical paths between a given cyclical set of nodes that generate the same $\Delta\gamma$ value. Finally, we have shown that the wave model correctly calculates $\Delta\gamma$ even though it considers only the starting and ending polarization states, and is entirely agnostic to notions of path. Thus, in this model, the notion of path memory is the same for both geometric phase and propagation phase.

Disclosures. The authors declare no conflicts of interest.

Data availability. In the paper's supplementary material, we include a Python script `draw_gamma_curves.py` (Code 1, Ref. [31]) that calculates the evolution curves of γ for each of the polarization state sequences considered in the paper, and a second Python script `draw_poincare_sphere_figures.py` (Code 2, Ref. [32]) for generating the Poincaré sphere figures used in Figs. 1–4.

REFERENCES

1. Y. Aharonov and J. Anandan, "Phase change during a cyclic quantum evolution," Phys. Rev. Lett. **58**, 1593–1596 (1987).
2. R. Nityananda and S. Sridhar, "Light beams with general direction and polarization: global description and geometric phase," Ann. Phys. **341**, 117–131 (2014).
3. C. P. Jisha, S. Nolte, and A. Alberucci, "Geometric phase in optics: from wavefront manipulation to waveguiding," Laser Photon. Rev. **15**, 2100003 (2021).
4. G. Giavarini, E. Gozzi, and D. R. W. D. Thacker, "On removing Berry's phase," Phys. Lett. A **138**, 235–241 (1989).

5. A. K. Pati, "Adiabatic Berry phase and Hannay angle for open paths," Ann. Phys. **270**, 178–197 (1998).
6. T. van Dijk, H. F. Schouten, W. Ubachs, *et al.*, "The Pancharatnam-Berry phase for non-cyclic polarization changes," Opt. Express **18**, 10796–10804 (2010).
7. J. C. Gutiérrez-Vega, "Pancharatnam-Berry phase of optical systems," Opt. Lett. **36**, 1143–1145 (2011).
8. L. Garza-Soto, N. Hagen, D. Lopez-Mago, *et al.*, "Wave description of geometric phase," J. Opt. Soc. Am. A **40**, 388–396 (2023).
9. M. Berry, "A geometric-phase timeline," Opt. Photon. News **35**, 42–49 (2024).
10. T. van Dijk, H. F. Schouten, and T. D. Visser, "Geometric interpretation of the Pancharatnam connection and non-cyclic polarization changes," J. Opt. Soc. Am. A **27**, 1972–1976 (2010).
11. J. Courtial, "Wave plates and the Pancharatnam phase," Opt. Commun. **171**, 179–183 (1999).
12. Z. Zhou, Y. Margalit, S. Moukouri, *et al.*, "An experimental test of the geodesic rule proposition for the noncyclic geometric phase," Sci. Adv. **6**, eaay8345 (2020).
13. M. V. Berry and S. Klein, "Geometric phases from stacks of crystal plates," J. Mod. Opt. **43**, 165–180 (1996).
14. A. Carollo, "The quantum trajectory approach to geometric phase for open systems," Mod. Phys. Lett. A **20**, 1635–1654 (2005).
15. C. Chryssomalakos, A. G. Flores-Delgado, E. Guzmán-González, *et al.*, "Curves in quantum state space, geometric phases, and the brachistophase," J. Phys. A **56**, 285301 (2023).
16. L. Palmieri, M. Cappelletti, M. Santagiustina, *et al.*, "Polarization-dependent phase of light propagating in optical fibers," J. Lightwave Technol. **41**, 6786–6794 (2023).
17. M. V. Berry, "Quantal phase factors accompanying adiabatic changes," Proc. R. Soc. London A **392**, 45–54 (1984).
18. A. Shapere and F. Wilczek, *Geometric Phases in Physics* (World Scientific, 1989).
19. J. Anandan, "Non-adiabatic non-abelian geometric phase," Phys. Lett. A **133**, 171–175 (1988).
20. A. Bohm, L. J. Boya, and B. Kendrick, "Derivation of the geometrical phase," Phys. Rev. A **43**, 1206–1210 (1991).
21. S. Pancharatnam, "Generalized theory of interference, and its applications. Part I: coherent pencils," Proc. Indian Acad. Sci. A **44**, 247–262 (1956).
22. D. Kestner and A. Kostinski, "Simple formula for the Jones product and the Pancharatnam connection in optics," Phys. Rev. A **109**, 023517 (2024).
23. R. A. Chipman, W.-S. T. Lam, and G. Young, *Polarized Light and Optical Systems* (CRC Press, 2019).
24. L. Garza-Soto, N. Hagen, D. Lopez-Mago, *et al.*, "Differences between the geometric phase and propagation phase: clarifying the boundedness problem," Appl. Opt. **63**, 645–653 (2024).
25. R. C. Jones, "A new calculus for the treatment of optical systems. VII. Properties of the N-matrices," J. Opt. Soc. Am. **38**, 671–685 (1948).
26. L. Garza-Soto, N. Hagen, and D. Lopez-Mago, "Deciphering Pancharatnam's discovery of geometric phase: retrospective," J. Opt. Soc. Am. A **40**, 925–931 (2023).
27. M. V. Berry, "Budden & Smith's 'additional memory' and the geometric phase," Proc. R. Soc. London A **431**, 531–536 (1990).
28. J. Anandan, "The geometric phase," Nature **360**, 307–313 (1992).
29. M. Ericsson, A. K. Pati, E. Sjöqvist, *et al.*, "Mixed state geometric phases, entangled systems, and local unitary transformations," Phys. Rev. Lett. **91**, 090405 (2003).
30. A. Alizzi, Z. K. Silagadze, and A. Uskov, "Berry phase of spin-one system in a rotating electric field," Eur. J. Phys. **45**, 025402 (2023).
31. N. Hagen, "Code for drawing geometric phase evolution curves," figshare (2024), https://doi.org/10.6084/m9.figshare.26420455.
32. N. Hagen, "Code for drawing paths on the Poincaré sphere," figshare (2024), https://doi.org/10.6084/m9.figshare.26420452.